

Magnetic anisotropy of FePt nanoparticles

Alamgir Kabir^a, Jun Hu^b, Volodymyr Turkowski^a, Ruqian Wu^b and Talat S. Rahman^a

^a Department of Physics, University of Central Florida, Orlando, FL 32816

^b Department of Physics and Astronomy, University of California, Irvine, Ca 92697

ABSTRACT. We carry out a systematic theoretical investigation of Magneto Crystalline Anisotropy (MCA) of $L1_0$ FePt clusters with alternating Fe and Pt planes along the (001) direction. The clusters studied consist of 1(2), 2(3), 3(4), and 4(5) layers of Fe(Pt), and vice versa. We calculate the structural relaxation and magnetic moment of each cluster by using *ab initio* spin-polarized density functional theory (DFT), and the MCA with both spin-polarized DFT (including spin-orbit coupling self-consistently) and the torque method. We find that the MCA of any composite structure of a given size is enhanced with respect to that of the same-sized pure Pt or pure Fe cluster as well as to that of any pair of Fe and Pt atoms in bulk $L1_0$ FePt. This enhancement results from the hybridization we observe (in company with other investigators) between the 3d orbital of the Fe atoms and the 5d orbital of their Pt neighbors. This hybridization, however, affects the electronic properties of the component atoms in significantly different ways. While it somewhat increases the spin moment of the Fe atoms, it has little effect on their orbital moment; at the same time, it greatly increases both the spin and orbital moment of the Pt atoms. Given the fact that the spin-orbit coupling (SOC) constant of Pt is about 7 times greater than that of Fe, this Fe-induced jump in the orbital moment of the Pt atoms produces the increase in MCA of the composite structures over that of their pure counterparts. That any composite structure exhibits higher MCA than bulk $L1_0$ FePt results from the lower coordination of Pt atoms in the cluster, whether Fe or Pt predominates within it. We also find that bipyramidal clusters whose central layer is Pt have higher MCAs than their same-sized counterparts whose central layer is Fe. This results from the fact that Pt atoms in such configurations are coordinated with more Fe atoms than in the latter. By thus participating in more instances of hybridization, they contribute higher orbital moments to the overall MCA of the unit. Our findings suggests that one can avoid necessity to encapsulate the FePt $L1_0$ nanoparticles in order to protect or enhance a high and stable magnetic anisotropy (mostly possessed by shell layers in the cuboctahedral case^{52,51}) by properly tailoring their structure.

Introduction

Understanding the physics of smaller structures can help in exploiting their useful properties. For example, the high surface-to-volume ratio and tailorable surface chemistry of metal nanoparticles have long been relied on in optimizing the activity and specificity of catalysts.¹ And small metal-particle arrays have been used to build single-electron devices.^{2,3} Recently demand has arisen for magnetic particles with high anisotropic energy necessary for energy-harvesting technologies⁴ as well as for ultra-high-density recording media.⁵ Satisfaction of this demand

requires development of metal thin-film media with smaller particles, more tightly-sized distributions, and optimized compositions.^{6,7}

Since the mid-1930s Fe-Pt alloys of L1₀ phase have been known to exhibit high magnetocrystalline anisotropy.⁸ Since among the various ferromagnetic metals and alloys FePt alloys show large perpendicular MCA (on the order of meV/atom⁹) and since, in nanoscale particles, they do not exhibit the superparamagnetism often characteristic of such small clusters,¹⁰ it lends itself to magnetic applications requiring small-grained constructions. FePt alloys also have advantages over rare-earth transition-metal-based compound with high MCA, such as Nd₂Fe₁₄B and SmCo₅ in that they are very ductile and chemically inert.¹¹ L1₀-based thin films and nanoparticles in general would seem to be promising candidates for ultra-high density magnetic storage media owing to their high corrosion resistance and excellent intrinsic magnetic properties.¹² But, in contrast to the fine grain of the L1₀ FePt systems, other conventional magnetic materials (Fe, Co, Ni and their alloys) would, through thermal fluctuation, within a very short time become superparamagnetic, losing any stored information. And given their high cost, bulk FePt-based permanent magnets can be used only for some especially delicate applications, as in magnetic micro-electromechanical systems (MEMS),¹³ and in dentistry as attachment devices for retaining a dental cap in the cavity.¹⁴

The chemically ordered FePt L1₀ structure can be obtained by annealing from the FCC structure of FePt alloy or by deposition on substrate above the L1₀ ordering temperature.^{15,16} At high temperature an FCC solid solution of Fe-Pt is observed in the A1 phase; below 1573K (and down to 973K) alloys with a nearly equal number of Fe and Pt atoms (35-55% Pt) show order disorder transition and the L1₀ ordered phase begins to form.¹¹ Though the L1₀ phase is typically obtained by heat treatment of A1 phase, it can also be produced by chemical synthesis of nanoparticles.¹² Deposition of alternate Fe and Pt monolayers can reduce the onset temperature of L1₀ phase.¹⁷ Another way to obtain L1₀ phase experimentally is by annealing alternating multi-layers of Fe and Pt.¹¹ Stable FePt L1₀ nanoparticles have been prepared experimentally in works [50] and [51] (capped with Al in the latter instance).

The L1₀ structure has alternating Fe and Pt planes along the (001) direction, which is also the easy axis of magnetization, abandoning the cubic symmetry of the FCC system. In this type of layered magnetic system the MCA is mainly due to the contribution from the Pt (5d element) having large spin-orbit coupling while the Fe (3d element) provides the exchange splitting of the Pt sub-lattice.¹⁸⁻²⁰ It is well known that in the FePt system, the Pt atoms play an important role in magnetic anisotropy, because the hybridization of Fe orbitals cause spin polarization of Pt atoms, which in turn enhance the MCA owing to the relative strong SOC of the Pt atoms in comparison with that of the Fe atoms.

There have been several theoretical studies on MCA of nanoparticles. Cyrille *et al.*²¹ present a size- and shape-dependent magnetic properties of L1₀ FePt clusters using a tight-binding approach. In their study the central plane of clusters is always Fe and they do not take into

account the atomic relaxation of the clusters. Błonski and Hafner²² undertook *ab initio* density-functional calculations of the magnetic anisotropy of supported nanostructures. Fernandez-Seivane and Ferrer²³ studied the correlation of the magnetic anisotropy with the geometric structure and magnetic ordering of small atomic clusters of sizes up to 7 atoms. Gruner *et al.*^{50,52} demonstrated that in cuboctahedral nanoparticles the high anisotropy of the layers increases as one moves towards the surface, and the anisotropy can be even enhanced by embedding the material in some suitable other metal (e.g., Au in the case of Pt-terminated structures).

Various experimental studies, using X-ray Magnetic Circular Dichroism Spectroscopy (XMCD) or X-ray Absorption spectra (XAS), have recently confirmed the enhancement of MCA in free or supported clusters.²⁴⁻²⁶

In the study reported here we carry out a systematic theoretical investigation of the MCA of L1₀ FePt clusters consisting of alternating Fe and Pt planes along the (001) direction, of sizes 30, 38, 71, 79, 114 and 140 atoms (both with Pt outer layers and with Fe outer layers), as well as that of the pure Fe and Pt clusters of same sizes. The clusters studied have 1(2), 2(3), 3(4) and 4(5) layers of Fe(Pt) atoms – both with Pt outer layers and with Fe outer layers – of sizes 30, 38, 71, 79, 114, and 140 atoms, respectively, . We also examine the electronic properties (including the orbital moments) of each atom in each of these configurations.

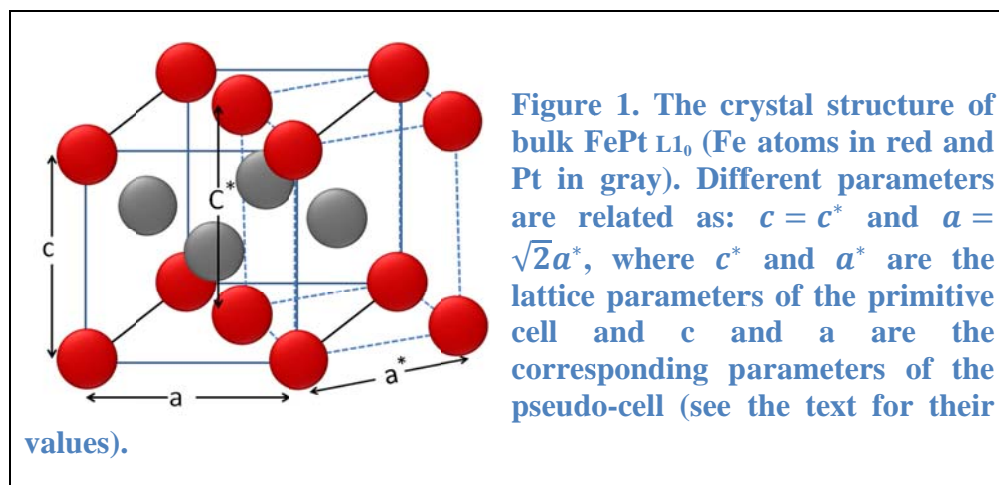
To calculate the structural relaxation and magnetic moments of the clusters we adopted an *ab initio* spin-polarized density functional theory (DFT) approach; to calculate their MCA employed two different methods: (i) a spin-polarized DFT with self-consistently included spin-orbit coupling and (ii) the torque method.

We found that the MCA of layered L1₀ FePt clusters is enhanced over that of both bulk FePt L1₀ and that of either a pure Fe or Pt cluster of comparable size. . Previous investigations attributed this enhancement is due to the hybridization 3d orbital of Fe atom with the 5d orbital of Pt atom. Our calculations indicate that this is so because this hybridization increases both spin and orbital moment of the Pt atoms. And given the large spin-orbit coupling constant of Pt it is this enhanced orbital moment of Pt that is responsible for the higher anisotropy of the system as a whole. We also found that when the central layer of the bipyramidal cluster is Pt the cluster has higher MCA than a cluster of the same size but with Fe as the central layer, in contrast to the cuboctahedral cases,^{50,52} in which it is the surface layers that exhibit higher MCA. This stems from the fact that when Pt atoms comprise the central layer they have more Fe atoms neighboring them, so that hybridization increases, lending them higher orbital moments than are possessed by Pt atoms in other layers. This center-of-system ‘concentration’ of the MCA makes it possible to preserve the anisotropy without having to resort to capping o the particles.

Computational details

To calculate the structural relaxation and spin and orbital magnetic moments we used the *ab initio* spin-polarized DFT approach implemented in the VASP code.¹ In describing the electronic exchange and correlation effects we used the spin-polarized generalized-gradient approximation (GGA) with the Perdew-Burke-Ernzerhof (PBE) functional² and the spin interpolation proposed by Vosko *et al.*³ In calculating the ionic relaxation, we employed the conjugate gradient algorithm. In describing the electron-ion interaction we used the projector augmented-wave (PAW)⁴ formalism. To calculate the strength of the spin-orbit coupling it is essential to take relativistic effects into account. We did so by choosing the relativistic version of PBE as an input to the noncollinear mode framework implemented in VASP.^{5,6}

To construct the bulk FePt L1₀ structure we replaced every alternating layer of FCC Fe with Pt atoms in (001) planes. This ordering induces a contraction along the (001) direction of the FCC lattice, which reduces the ratio c^*/a^* , where a^* is the nearest-neighbor distance in (001) planes (related to the primitive cell parameter a as $a = \sqrt{2}a^*$), from the FCC value ($\sqrt{2}$) to 1.363. Fig. 1 shows the relation between the lattice parameter for the pseudo-cell and the parameter for the primitive unit cell.



Lattice distortion brings about chemical re-ordering in the in the unit cell. For the lattice parameter we used the experimentally-derived data for bulk powder,¹⁰ ($a^*=2.72\text{\AA}$ and $c^*/a^* = 1.36$), and then relaxed the structure using the DFT approach described above.

To obtain the relaxed geometry of a cluster of given size and shape, we first obtained the relaxed lattice parameter for bulk L1₀ FePt, then cut the bulk to the size and layered shape of the cluster in question to get its initial configuration, and finally relaxed that configuration. In calculating the MCA of L1₀ FePt nanoparticles we used both the direct⁷ method (i.e., including spin-orbit coupling self-consistently), and the torque^{8,9} method.

Results

Magnetic anisotropy of the bulk system

The lattice parameters of the relaxed structure of bulk L1₀ FePt do not change much from the experimental one ($a^*=2.72\text{\AA}$ and $c^*/a^* = 1.36$): the in-plane parameter $a^*=2.74\text{\AA}$, and the ratio value $c^*/a^* = 1.37$. We have obtained the following values for the magnetization: $2.85\mu_B$ for the Fe atoms and $0.36\mu_B$ for the Pt atoms, both in good agreement with experiment (Fe: $2.90\mu_B$, Pt: $0.34\mu_B$).¹⁰ It is worth mentioning that though bulk Pt is nonmagnetic, in the FePt alloy Pt atoms possess magnetic moment, while the magnetic moment of Fe atoms magnetic moment increases only slightly in the alloy from their values in bulk Fe. The enhancement of the Fe magnetic moment is a consequence of the hybridization between the states of the 3d orbitals of the Fe atoms and the not only the 5d but also s- and p-orbitals of their neighboring Pt atoms. As can be seen in Fig. 2, the hybridization causes a broadening of the d-bands for the majority spins, while its effect (broadening) on the minority spins is less significant. Thus, it is natural to suppose that the finite magnetic moment ($0.36\mu_B$) of Pt atoms in FePt clusters comes mostly from the hybridization of the minority spin bands.

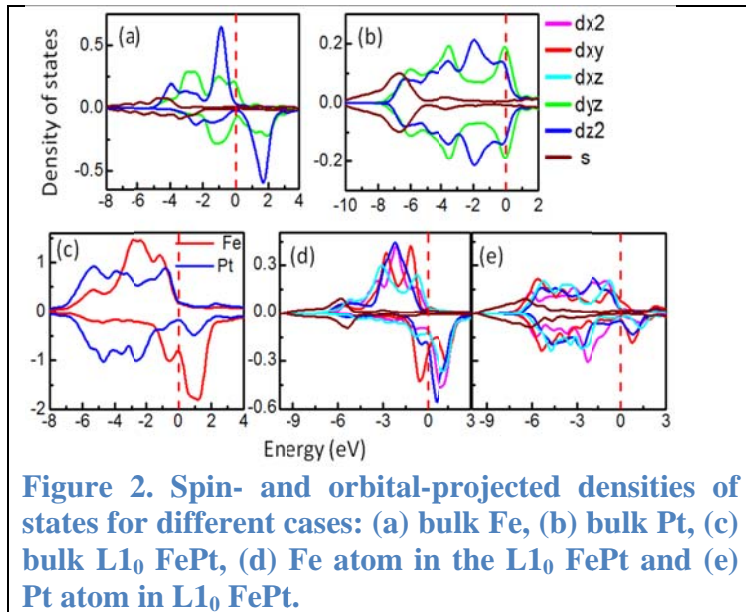


Figure 2. Spin- and orbital-projected densities of states for different cases: (a) bulk Fe, (b) bulk Pt, (c) bulk L1₀ FePt, (d) Fe atom in the L1₀ FePt and (e) Pt atom in L1₀ FePt.

The density of states (DOS) of bulk L1₀ FePt is plotted in Fig. 2, where we also present the projected DOS for the Fe and Pt atoms, which is similar to the one reported by C. Barreateau *et al.*

¹¹ Our calculations show MCA value for the bulk to be 2.22meV per FePt pair, which is also in agreement with other studies,¹² encouraging confidence that our results in the nanocase are

reliable as well. We attribute the large MCA to the large SO coupling of Pt atoms and to the increase in orbital moment owing to the strong hybridization of their $5d$ orbitals with the $3d$ orbitals of Fe. It is this hybridization that breaks the symmetry of free energy in the two perpendicular directions, resulting in a surplus of free energy in the direction of magnetization.¹³ Interestingly, Lyubina *et al.* found that the anisotropy of the disordered phase of FePt is an order of magnitude less than that of the $L1_0$ phase.¹⁴

Magnetic anisotropy of the dimer

To gain more insight into the nature of MCA in the larger systems, we have also considered the case of FePt dimer. We obtained a dimer bondlength of 2.184\AA when leaving spin-orbit coupling out of account, and 2.172\AA when taking spin-orbit coupling into account. We thus infer that spin-orbit coupling does not play an important role in determining the geometry of this system. This result is also in good agreement with the results of Ref. [36]. In addition, we have studied the properties of the pure Fe and Pt dimers. Fe_2 turns out to have a very small anisotropy owing to the small SOC in the Fe atom (6mRy). In the case of Pt_2 , both the magnetic and orbital moments change when the magnetic field is applied in different (x - and z -) directions, which causes a large MCA due to a large SOC of the Pt atom (40mRy) and larger anisotropy in orbital moments. The anisotropy of the mixed FePt system has value between those of the two monometallic systems (Table 1).

In the FePt dimer the magnetic moment of the Fe atom is $3.22\mu_B$ and of the Pt atom $-0.58\mu_B$. The large magnetic moment of Fe in this dimer can be caused by the charge transfer from the $3d$ orbital of Fe to the $5d$ orbital of the Pt atom, which creates a polarization and an extra “hole charge” on the Fe atom.¹⁵ The MCA for FePt dimer is 3.76meV perpendicular to the dimer axis. This value is higher than the value for Fe_2 , because the values of both the spin and orbital momenta are larger in the FePt dimer.

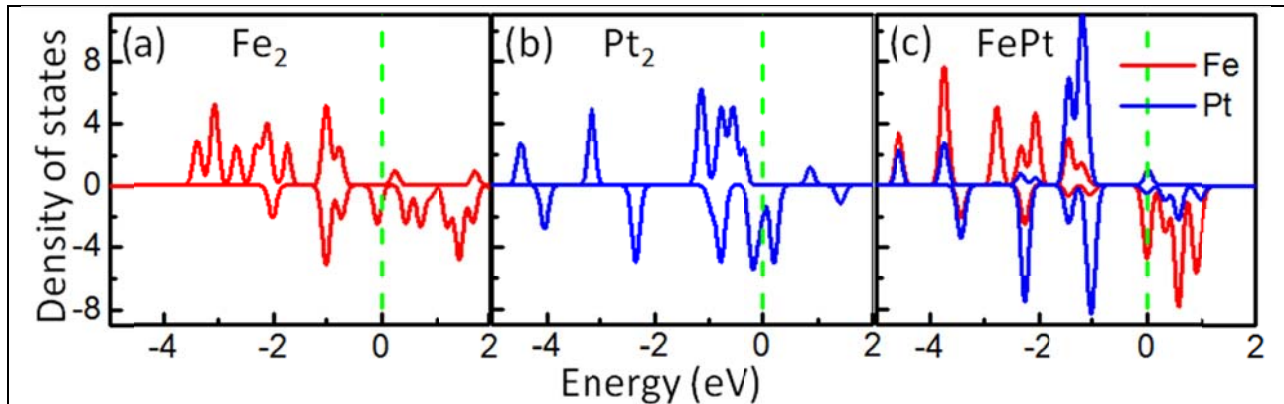
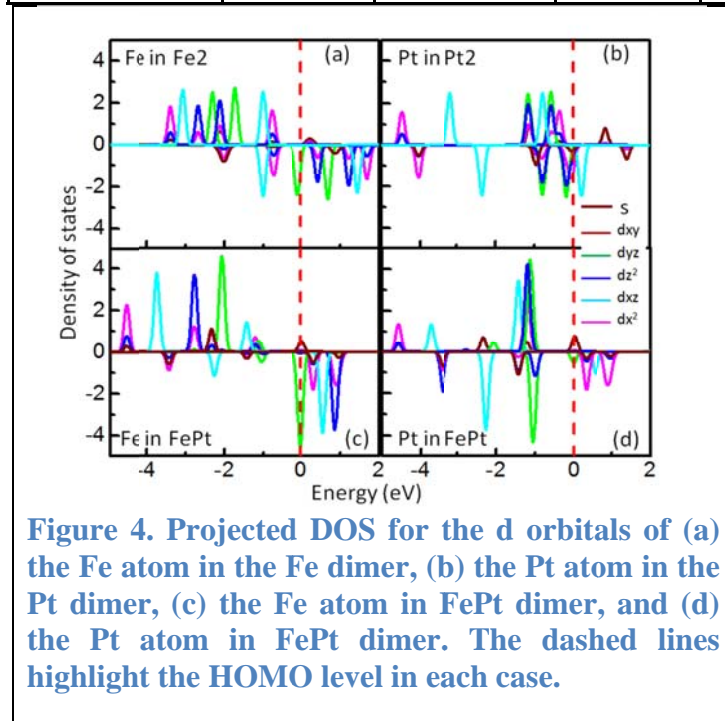


Figure 3. Density of states of (a) each Fe atom in the Fe dimer, (b) of each Pt atom in the Pt dimer and (c) of the Fe and Pt atoms in the FePt dimer. The red line corresponds to Fe atoms and the blue line to Pt atoms. The dashed green lines indicate the HOMO level of the dimers.

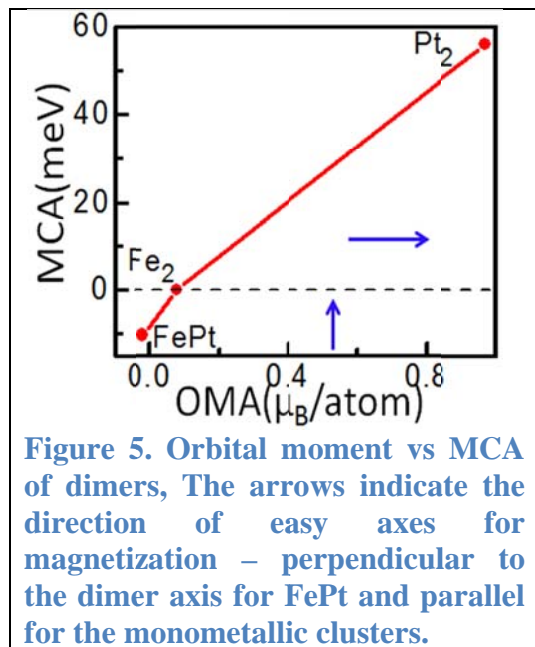
In all three cases, the easy axis of magnetization coincides with the direction of highest orbital momenta, in agreement with the Bruno's model¹⁶ (See Table 1). The negative value of MCA (for the FePt dimer) corresponds to the case of the easy axis of magnetization perpendicular to the dimer axis.

Table 1: Magnetic moments and MCA energy of the Fe, Pt and FePt dimers.

	Magnetic Moment (μ_B)		Orbital Moment (μ_B)		MCA (meV)
	(100) direction	(001) direction	(100) direction	(001) direction	
Fe ₂	5.99	5.99	0.32	0.16	0.07
Pt ₂	1.8938	1.3843	2.737	0.798	55.94
FePt	4.16	4.26	0.362	0.407	-10.37



The projected DOS for the *d* orbitals of the Fe and Pt atoms in the dimers are shown in Fig.4. As follows from this figure, the majority spin orbitals have zero occupancy at the HOMO level, but the minority spins are present there, indicating that the change of the orbital occupancy upon hybridization is defined by the charge transfer for the spin-down electrons only. We thus conclude that the anisotropy and the magnetization of the dimers are defined by the minority spins as well.



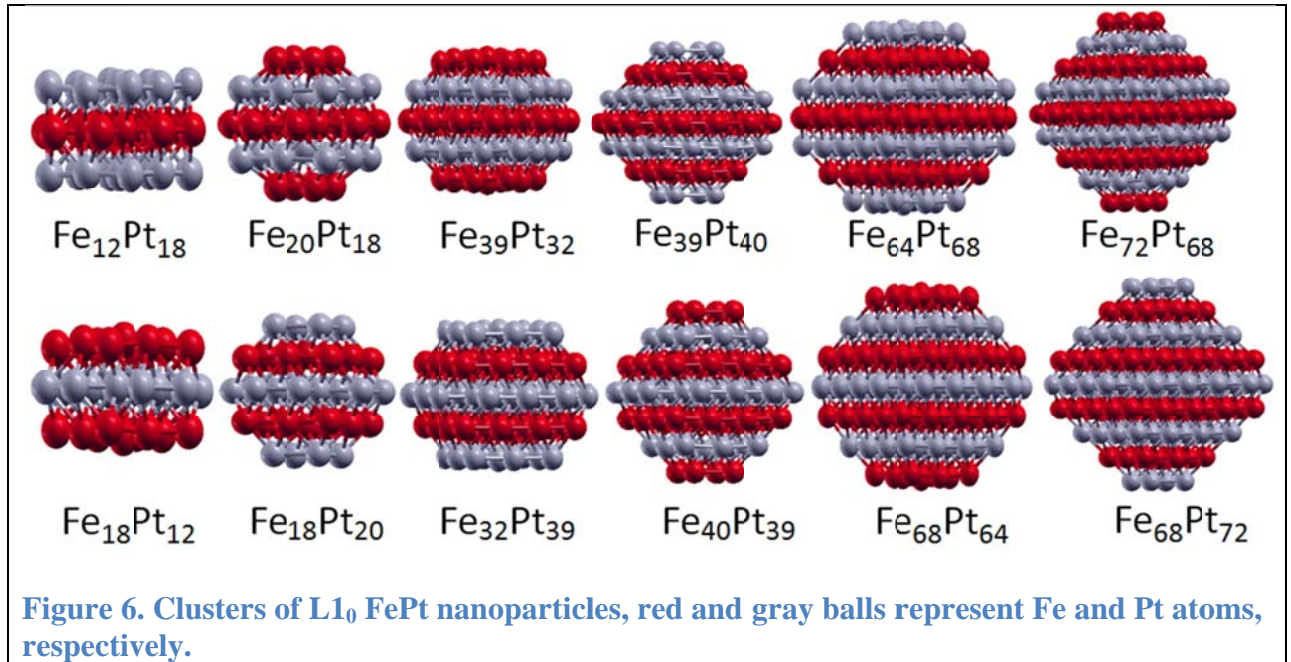
To summarize: assuming that the MCA is proportional to the change of orbital momentum in two different directions, the comparatively small value of MCA for Fe₂ is due to its small SOC constant; larger value of MCA for Pt₂ is due to its large SOC constant. In this case, quite predictably, the mixed system of FePt dimer has MCA with its value between the values for two pure dimers.

Magnetic anisotropy of L1₀ FePt nanoclusters

For the high MCA of bulk L1₀ FePt alloys with the equiatomic composition stimulated the researchers to look in the direction of smaller size particles. Though there are some problems regarding this, for example Muller et al. predicted theoretically that L1₀ phase is not stable thermodynamically¹⁷, and another study by Jarvi et al.¹⁸ showed that the structure may alternate the arrangement of atomic order. Also, several experimental studies support the existence of a minimum particle size below which the L1₀ order can no longer be achieved,^{19,20} and many other studies showed the segregation of Pt atom to the surface for smaller size of particles.^{21, 22} However, to get final answer on possibility of applications of FePt structures in the applications mentioned above need more detailed and thorough studies. In particular, it is known that the magnetic properties of nanoparticles depend on the size, shape and the way of synthesizing.¹⁴ Gas phase particles can have MCA lower than the bulk perfectly ordered L1₀ alloys, because (i) the structure may not be perfect L1₀, and can have lots of multiply twined particles, (ii) the Pt atoms may be segregated on the surface.^{43,44} or (iii) an inhomogeneous alloying may take place,

as indicated by the EXAFS measurements by Antioniak.²³ The enhancement of surface to volume ratio of a nanoparticle plays a significant role on MCA and so thus the size of the particles. For example the crystal symmetry-related quenching of the orbital magnetic moments is lifted for any surface atoms of nanoparticles, thereby causing an enhancement of orbital moment of the surface atoms compared to the bulk or core atoms.²⁴ Fe orbital moments of surface atoms in L1₀ FePt nanoparticles showed larger values of OM than the surface atoms, as it shown in the other XMCD measurements by Antioniak.²⁵

As we mentioned above, the initial configuration of L1₀ nanoparticles was obtained by cutting the relaxed bulk FePt L1₀ structure. We have considered the cases of the 30-, 38-, 71-, 79-, 114-, and 140- atom nanoparticles with alternating Fe and Pt layers, and also pure Fe and Pt clusters with the same structures. All the calculations is done by using one (Gamma) point in the Brillouin Zone, and the size of the supercell was chosen to be 12Å vacuum in all three directions to prevent artificial electric field interactions between images, similar to the dimer case. The cluster structures are shown in the Fig. 6.

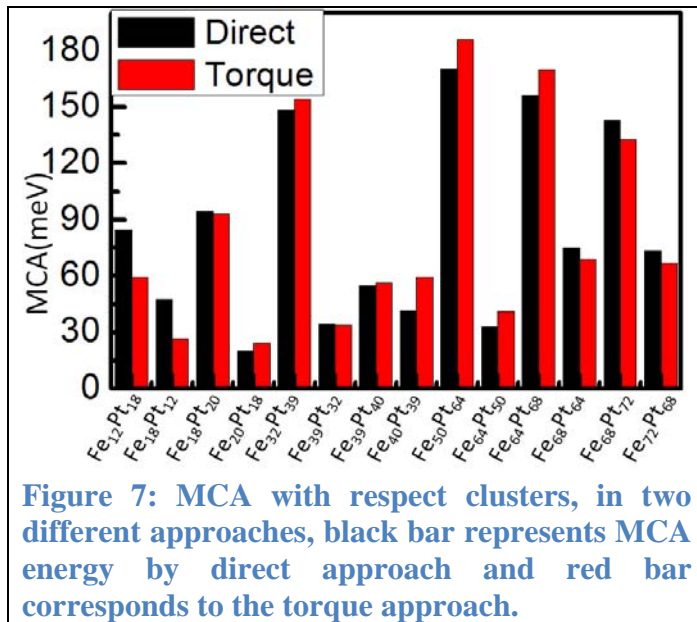


Once the structural relaxation is completed, the MCA is calculated by comparing band energy between two magnetic orientation, as

$$MCA = E(\uparrow) - E(\rightarrow) = \sum_{occ'} \varepsilon_i(\uparrow) - \sum_{occ''} \varepsilon_i(\rightarrow) \quad (1)$$

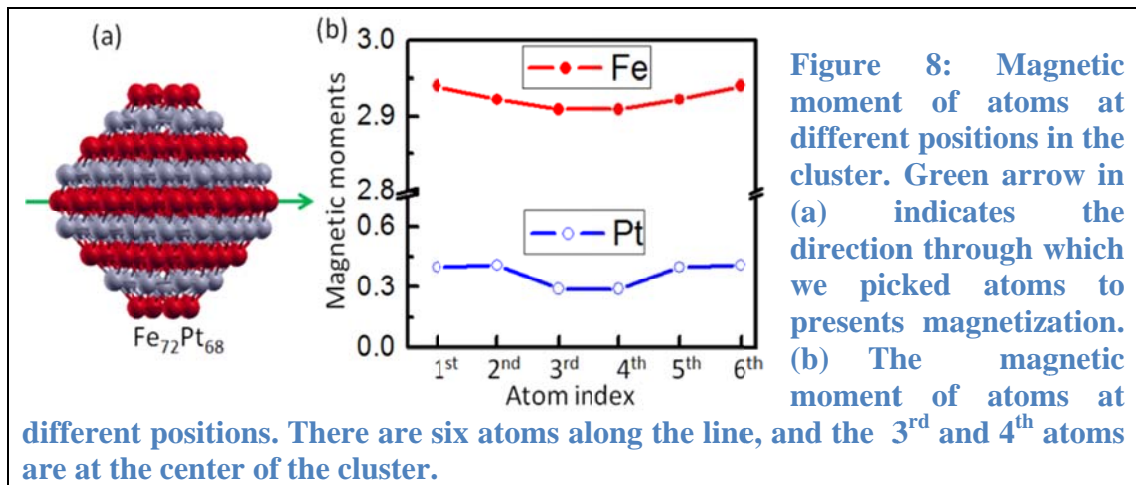
where ε_i is the band energy of the i^{th} state and the arrow in the parentheses denote the direction of magnetization (it is usually the direction parallel and perpendicular to the surface of a film,

and for nanoparticles it is parallel to xy-plane and along z-axis). The band energy of the system can be calculated by using spin-polarized DFT with or without SOC taken into account, since MCA is the ground state property of the system. The magnetization was aligned towards two specific directions by using non-collinearity of spin arrangement in the system. The sums in equation (1) are usually large numbers (on the order of hundreds of eV), whereas the MCA is on the order of few meV, so MCA is a small number coming from the difference of two large numbers. For this reason, one needs to be very careful about the convergence of calculation while determining the Kohn-Sham energy of the system. In fact, it is necessary to use very fine K-point mesh in the reciprocal space for accurate integration. A very accurate convergence of energy is also required in the SCF cycle, which makes the calculations rather expensive. This method may give contradictory results if one does not use sufficient number of integration points, for example Gay and Richter²⁶ predict the easy axis to be perpendicular to the plane of monolayer of Fe and found anisotropy energy of -0.4meV/atom, whereas Karas et al.²⁷ found the easy axis to be along the plane of the layer, and the value of anisotropy 3.4 meV/atom. Since we used a large supercell in the calculations, we do not need to include large number of K points, though we did a set of calculations for $3 \times 3 \times 3$ k-point mesh as a test for 38 atom clusters, and the results are almost same as in the case with $1 \times 1 \times 1$ k-points. Therefore, in other calculations we used $1 \times 1 \times 1$ k-point mesh only. The values of MCA for the above clusters obtained with both methods are presented in Fig. 7.



MCA with direct method and torque method agree well except for the smaller clusters (Fe₁₈Pt₁₂ and Fe₁₂Pt₁₈) clusters. In the last case, the direct method gives much higher MCA than the torque method. On the other hand, one can expect that the torque method is not very accurate in the case of small clusters, since the torque calculations depend upon the uniaxial symmetry of the system, and smaller clusters lose their symmetry. However, since there are no experimental values of

MCA in the case of such clusters, it is difficult to judge which method gives more accurate results. One definitive conclusion which comes from the calculations is that the nanoparticles with a larger number of Pt atoms have larger MCA. We also found that the atoms on the outside of the clusters have higher magnetic moments than the atoms inside. One example of such a situation is shown in Fig.8 for $\text{Fe}_{72}\text{Pt}_{68}$ and $\text{Fe}_{68}\text{Pt}_{72}$ clusters. The line through which we calculate the magnetic moment is presented by green arrow in Fig. 8(a). Red and blue in Fig. 8(b) represents magnetization for Fe (middle layer with Fe atoms, $\text{Fe}_{72}\text{Pt}_{68}$) and Pt (middle layer with Pt atoms, $\text{Fe}_{68}\text{Pt}_{72}$) atoms respectively. It is clear from the Figure that the outer atoms in the cluster have larger magnetization than the inner atoms, which may be explained by different number of neighbors in two cases.



Pt atoms in the FePt clusters are showing magnetization unlike the bulk Pt. This is due to the orbital hybridization of Pt with Fe atoms. Once again, the inside Pt atoms have smaller magnetization compared to the Pt atoms outside, and same is true for the Fe atoms. The reduced number of neighbors for the surface atoms can be regarded as a reason for a narrowing of the 3d(5d) orbital “bands” for the Fe(Pt), which may cause the enhancement of the magnetization of the surface atoms.

The projected DOS for the atoms at different positions in the clusters is presented in Fig. 9.

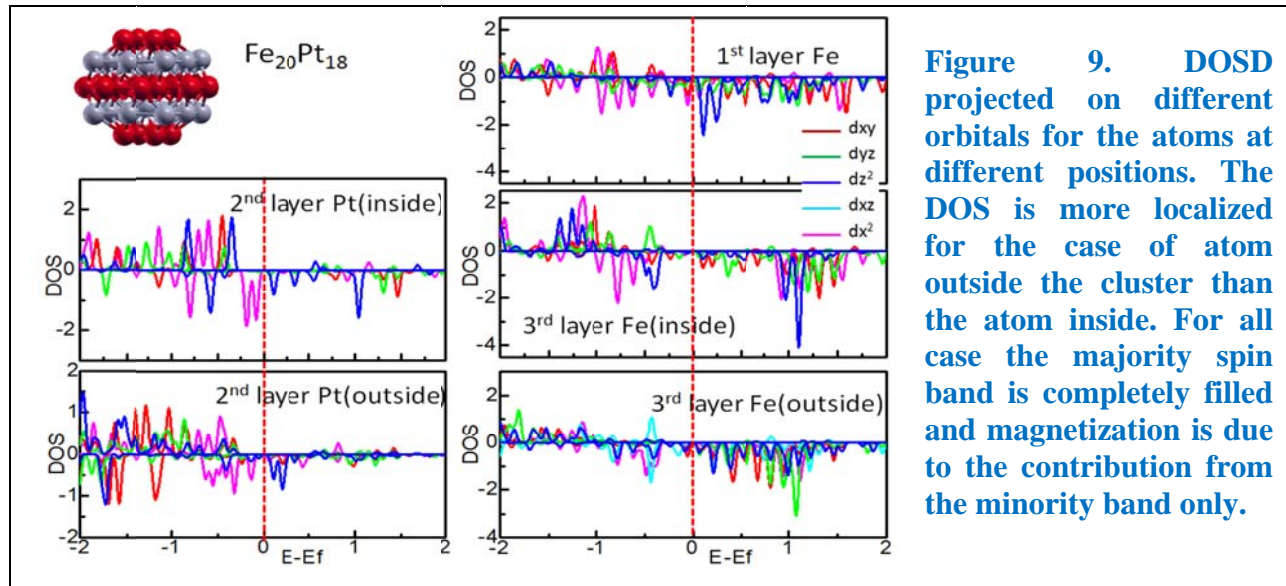


Figure 9. DOS projected on different orbitals for the atoms at different positions. The DOS is more localized for the case of atom outside the cluster than the atom inside. For all case the majority spin band is completely filled and magnetization is due to the contribution from the minority band only.

As it follows from this Figure, the projected PDOS of the Pt atoms is very similar for the spin-up and spin-down electrons, while there is a significant difference in DOS for the atoms inside and outside of the cluster. The PDOS of Fe atom outside the clusters are more spread then the PDOS of the Fe atom inside the cluster and the difference between the up- and down-spins is larger for the outside atoms. In all cases, the majority-spin states are completely filled, so the MAE is defined by the minority spin states only.

Table 2: The magnetic moments, orbital moments, and MCA of clusters along two different directions.

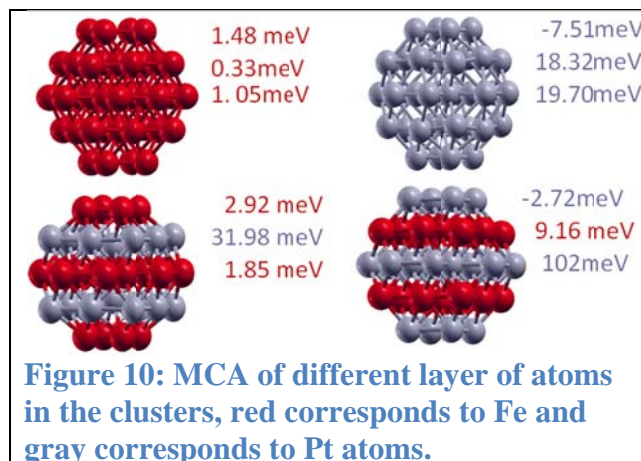
	Magnetic Moment (μ_B)		Orbital Moment (μ_B)		MAE
	Mx	Mz	Lx	Lz	MAE=(Ex-Ez)
Fe ₁₂ Pt ₁₈	46.74	46.26	2.283	2.037	84.60
Fe ₁₈ Pt ₁₂	62.33	62.03	2.14	2.54	47.60
Fe ₁₈ Pt ₂₀	68.16	68.06	3.311	2.968	94.37
Fe ₂₀ Pt ₁₈	72.76	72.75	3.304	3.092	20.01
Fe ₃₂ Pt ₃₉	117.18	115.19	5.860	4.461	154.28
Fe ₃₉ Pt ₃₂	134.18	134.14	5.393	5.221	34.15
Fe ₃₉ Pt ₄₀	133.57	132.46	5.737	5.170	81.05
Fe ₄₀ Pt ₃₉	137.26	136.53	6.130	5.630	71.82
Fe ₅₀ Pt ₆₄	175.97	175.67	7.948	6.911	170.11

Fe ₆₄ Pt ₅₀	213.24	213.44	8.515	7.910	33.33
Fe ₆₄ Pt ₆₈	214.84	214.76	9.638	8.241	155.90
Fe ₆₈ Pt ₆₄	232.88	232.64	10.084	9.112	75.06
Fe ₆₈ Pt ₇₂	233.90	231.71	10.586	10.060	142.80
Fe ₇₂ Pt ₆₈	242.69	242.95	10.154	10.507	73.65

The spin moment and orbital momenta were calculated by taking into account the SOC. As it follows from Table 3, the total magnetic moment doesn't significantly change for changing direction of magnetization from (001) to the (100). The orbital moment changed in such a way that the easy axis of magnetization is always along the direction of lower orbital moments, which contradicts with Bruno's model¹⁶ results, that the easy axis of magnetization always coincides with the direction of the highest orbital moments. So, in the case of dimer the direction of easy magnetization follows the direction of highest orbital moment of the system, but for larger clusters it follows the opposite trends. This suggests that one may expect a rotation of easy axis of magnetization from smaller to larger size of the clusters.

The change in orbital moments $\Delta L=L_x-L_z$ per atom with respect to the MCA of the clusters is presented in Fig. 7. The clusters with highest change of the orbital moments per atom have the highest anisotropy, which is in agreement with Table 3 results. Therefore, the contribution to MAE comes mostly from the change in orbital moment of the system and hence spin-orbit coupling energy.

We also studied the MAE of different layers on the clusters (Fig. 10).



As it follows from the Fig. 10, the system with central Pt plane has much higher anisotropy comparing to than the one with central Fe atoms. We found this is also true for all the other clusters we studied. This can be explained as follows. When the Pt atom is hybridized with Fe

atom in FePt clusters, the orbital moment of Pt atoms got changed. In $\text{Fe}_{20}\text{Pt}_{18}$ cluster Pt atom shows an orbital moment of $0.11\mu_B$ whereas when it is in $\text{Fe}_{18}\text{Pt}_{20}$ clusters the orbital moments of Pt increases to $0.15\mu_B$ (Table. 4). This increase of the orbital moments leads to a stronger higher spin-orbit coupling energy, and thus increases the MAE of the central layer.

Table 3: Orbital moments per atom in different clusters. Red color is used to emphasize a large change of orbital moments of Pt atoms in FePt L1₀ clusters.

Fe ₃₈	Pt ₃₈	Pt atom in Fe ₂₀ Pt ₁₈	Fe atom in Fe ₂₀ Pt ₁₈	Pt atom in Fe ₁₈ Pt ₂₀	Fe atom in Fe ₁₈ Pt ₂₀
0.06	0.02	0.110	0.06	0.145	0.04

Pure Fe and Pt L1₀ clusters have very small orbital moment, for Fe it is $0.06\mu_B$ per atom and for Pt is $0.02\mu_B$, but in the FePt L1₀ clusters Pt atoms always have large orbital moments comparing to the Fe atom as can be seen from Table 3. The difference in anisotropy for different layers of Fe/Pt atoms can be explained by using a perturbation theory calculations, since the SOC part of the Hamiltonian is much smaller than the d bandwidth.⁴⁸ It is seen from the Fig. 11 that all the majority spin states are completely occupied, so the empty states belongs to the minority spins only. Since there is not any empty states for the spin-up electrons, there are only two types of SO interactions in the systems: the coupling between occupied and unoccupied spin down states and the coupling between the occupied spin-up with unoccupied spin-down electrons. The MCA energy can be calculated in the perturbation theory approach by using the following formula:⁴⁸

$$E_x - E_z \sim \xi^2 \sum_{o,u} \frac{|\langle o|L_z|u\rangle|^2 - |\langle o|L_x|u\rangle|^2}{\epsilon_u - \epsilon_o},$$

where $\langle o|$ and $\langle u|$ are the occupied and unoccupied minority spin states, respectively, and L_z and L_x are the z and x component of the angular momentum operators. We have calculated the orbital occupancy of both empty and filled states of both spin arrangement and found that for the Fe atom in the 1st layer of $\text{Fe}_{20}\text{Pt}_{18}$ $E_x - E_z = 0.51\xi^2$ (ξ is the spin-orbit coupling), and for the atoms in the 3rd layer of $\text{Fe}_{20}\text{Pt}_{18}$ this value is $E_x - E_z = 0.26\xi^2$.

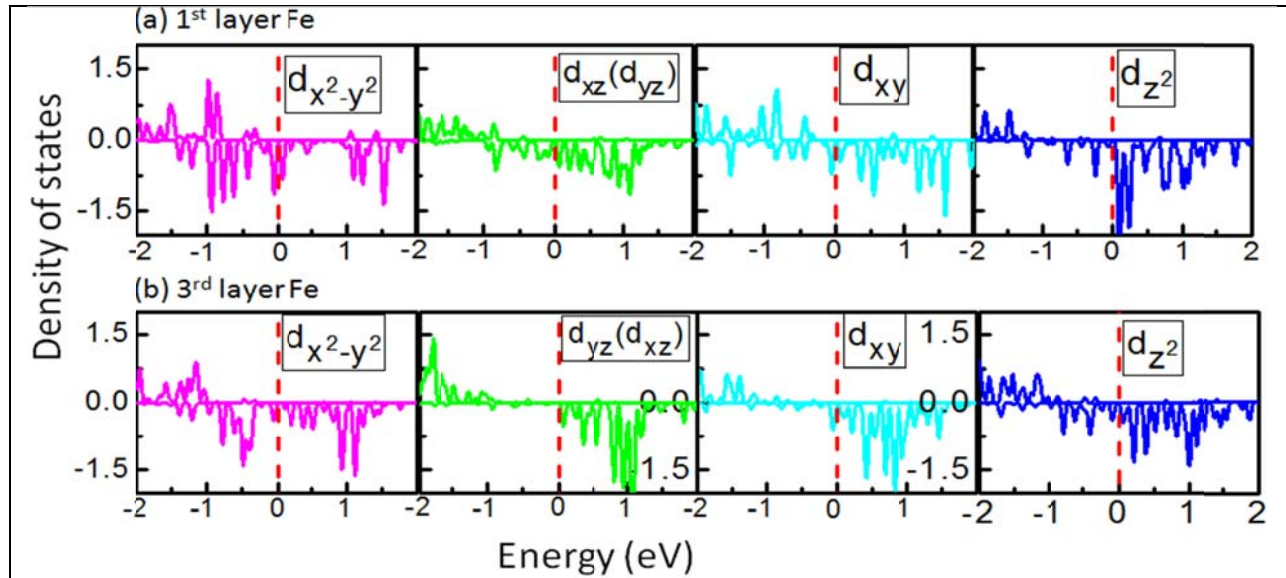


Figure 11. Projected DOS for the Fe atom (a) in the 1st layer, and (b) in the 3rd layer of the Fe₂₀Pt₁₈ cluster.

Since contribution of SOC is lower by half for 3rd layer atom than 1st layer atom, one can expect that the anisotropy for the 1st layer would be double than that for the 3rd layer. In our case, this value is higher than double (three times), which may come from the simplicity of the estimation used. In particular, one needs to take into account the difference in hybridization for individual atoms. One example of the orbital occupancy for different atoms is given in the Table 4.

Table 4: Occupancy of d-orbitals of some of the Fe atoms in the Fe₁₈Pt₂₀.

	1 st layer atom	3 rd layer atom
$d_{x^2-y^2}$	0.51	0.45
d_{xy}	0.29	0.17
d_{xz}, d_{yz}	0.30	0.10
d_{z^2}	0.18	0.28

Conclusions

We have systematically studied the magnetic properties of L1₀ nanoparticles as a function of particle sizes (30, 38, 71, 79, 114 and 140 atoms) and compositions (i.e., consisting of pure Fe and Pt atoms and of alternating planes of Fe and Pt atoms). We find that nanoparticles have much higher magnetic moments than do bulk atoms. This is due to the fact that the MCA arises from the orbital moment coupled with the spin moment and that in the bulk the system orbital moments are almost quenched, whereas in small clusters the orbital moments of the system's

atoms are considerably enhanced. We propose that this explains why it is that (as earlier studies have shown) the hybridization of the $5d(Pt)$ orbitals with $3d(Fe)$ orbitals produces a high magnetic anisotropy for layered FePt nanoparticles. We also find that clusters with Pt atoms as the central layer have much larger anisotropy than those in which the central layer consists of Fe atoms. The explanation for this is that the central layer has more atoms than other layers in the cluster, and when *these* atoms are of high orbital moment – Pt atoms hybridizing with the Fe atoms below and above – the system as a whole exhibits higher anisotropy than when its central layer consists of Fe atoms, whose orbital moment, in hybridizing with the Pt atoms above and below, is markedly lower. Contrary to the cubooctahedral case,^{50,52} the bipyramid nanoparticles possess MCA mostly at the (large) central Pt layer, which may remove the necessity to cap them in order to protect MCA. At the same time a deeper analysis of the electronic structure of these systems might be required in order to obtain more detailed understanding of their magnetic properties. In particular, the effects of strong electron correlations in these systems with localized d-orbitals in the cases of different sizes and geometries need to be studied (see, e.g., Refs. [53,54]).

While the stability of the relatively small clusters considered in this paper might be questionable, we hope that the theoretical insights here obtained can serve as a fruitful prompt for experimentalists in search of (larger) high-density nanoparticles exploitable in recording devices.

ACKNOWLEDGMENTS

We would like to thank Lyman Baker for critical reading of the manuscript and numerous enlightening comments. The work was supported in part by DOE Grant DE-FG02-07ER46354.

References

- ¹ A. T. Bell, *Science* **299**, 1688 (2003).
- ² R.P. Andres, T. Bein, M. Dorogi, S.Feng, J.I. Henderson, C.P. Kubiak, W. Mahoney, R. G. Osifchin, and R. Reifenberger, *Science* **272**, 1323 (1996).
- ³ D. Davidović and M. Tinkham, *Appl. Phys. Lett.* **73**, 3959 (1998).
- ⁴ N. Jones, *Nature* **472**, 22 (2011).
- ⁵ J. Henderson, S. Shi, S. Cakmaktepe, and T. M. Crawford, *Nanotechnology* **23**, 185304 (2012).
- ⁶ T. Yogi, C. Tsang, T. A. Nguyen, K. Ju, G.L. Gorman, and G. Castillo, *IEEE Trans. on Magn.* **26**, 2271 (1990).
- ⁷ J. S. Li, M. Mirzamaani, X.P. Bian, M. Doerner, S.L. Duan, K. Tang, M. Toney, T. Arnoldussen, and M. Madison, *Journ. of Appl. Phys.* **85**, 4286 (1999).
- ⁸ L. Graf and A. Kussmann, *Phys. Z.* **36**, 544 (1935).
- ⁹ C. Antoniak et al., *Phys. Rev. Lett.* **97**, 117201 (2006).
- ¹⁰ R. P. Cowburn, *Journ. of Appl. Phys.* **93**, 9310 (2003).

11 J. Lyubina, B. Rellinghaus, O. Gutfleisch, and M. Albrecht, Handbook of Magnetic
Materials Vol.19, p. 291 (Amsterdam: Elsevier, 2011).

12 S. Sun, C.B. Murray, D. Weller, L. Folks, and A. Moser, Science **287**, 1989 (2000).

13 B. Azzerboni, G. Asti, and L. Pareti, *Magnetic Nanostructures in Modern Technology:
Spintronics, Magnetic MEMS and Recording* (Springer, 2007).

14 I. Watanabe, Y. Tanaka, E. Watanabe, and K. Hisatsune, J. Prosthet. Dent. **92**, 278
(2004).

15 S. Okamoto, N. Kikuchi, O. Kitakami, T. Miyazaki, Y. Shimada, and K. Fukamichi,
Phys. Rev. B **66**, 024413 (2002).

16 J. U. Thiele, L. Folks, M. F. Toney, and D. K. Weller, Journ. of Appl. Phys. **84**, 5686
(1998).

17 G.H. Daalderop, P.J. Kelly, and M.F. Schuurmans, Phys. Rev. B **44**, 12054 (1991).

18 I.V. Solovyev, P.H. Dederichs, and I. Mertig, Phys. Rev. B **52**, 13419 (1995).

19 A.B. Shick and O.N. Mryasov, Phys. Rev. B **67**, **172407** (2003).

20 T. Shima, T. Moriguchi, S. Mitani, and K. Takanashi, Appl. Phys. Lett. **80**, 288 (2002).

21 P. Gambardella et al., Science **300**, 1130 (2003).

22 S. Rohart, C. Raufast, L. Favre, E. Bernstein, E. Bonet, and V. Dupuis, Phys. Rev. B **74**,
104408 (2006).

23 J. Miyawaki, D. Matsumura, H. Abe, T. Ohtsuki, E. Sakai, K. Amemiya, and T. Ohta,
Phys. Rev. B **80**, 020408(R) (2009).

24 C. Barreteau and D. Spanjaard, Journ. of Phys.: Cond. Mat.: **24**, 406004 (2012).

25 P. Blonski and J. Hafner, Journ. of Phys.: Cond. Mat. **21**, 426001 (2009).

26 L. Fernandez-Seivane and J. Ferrer, Phys. Rev. Lett. **99**, 183401 (2007).

27 G. Kresse and J. Hafner, Phys. Rev. B **47**, 558 (1993).

28 J.P. Perdew, J.A. Chevary, S.H. Vosko, K.A. Jackson, M.R. Pederson, D.J. Singh, and C.
Fiolhais, Phys. Rev. B **46**, 6671 (1992).

29 S.H. Vosko, L. Wilk, and M. Nusair, Can. Journ. of Phys. **58**, 1200 (1980).

30 G. Kresse and D. Joubert, Phys. Rev. B **59**, 1758 (1999).

31 D. Hobbs, G. Kresse, and J. Hafner, Phys. Rev. B **62**, 11556 (2000).

32 M. Marsman and J. Hafner, Phys. Rev. B **66**, 224409 (2002).

33 X. Wang, R. Wu, D. Wang, and A. J. Freeman, Phys. Rev. B **54**, 61 (1996).

34 R. Wu and A. J. Freeman, Journ. of Magn. and Magn. Mat. **200**, 498 (1999).

35 J. Lyubina, I. Opahle, M. Richter, O. Gutfleisch, K.-H. Müller, L. Schultz, and O. Isnard,
Appl. Phys. Lett. **89**, 032506 (2006).

36 K. Boufala, L. Fernández-Seivane, J. Ferrer, and M. Samah, Journ. of Magn. and Magn.
Mat. **322**, 3428 (2010).

37 P. Bruno, Physical Review B **39**, 865 (1989).

38 D. Weller and A. Moser, IEEE Transactions on Magnetism **35**, 4423 (1999).

39 M. Müller, P. Erhart, and K. Albe, Phys. Rev. B **76**, 155412 (2007).

40 T. T. Järvi, D. Pohl, K. Albe, B. Rellinghaus, L. Schultz, J. Fassbender, A. Kuronen, and
K. Nordlund, Europhys. Lett. **85**, 26001 (2009).

41 T. Miyazaki, O. Kitakami, S. Okamoto, Y. Shimada, Z. Akase, Y. Murakami, D. Shindo,
Y.K. Takahashi, and K. Hono, Phys. Rev. B **72**, 144419 (2005).

42 Y.K. Takahashi, T. Koyama, M. Ohnuma, T. Ohkubo, and K. Hono, Journ. of Appl.
Phys. **95**, 2690 (2004).

- 43 R.M. Wang, O. Dmitrieva, M. Farle, G. Dumpich, H.Q. Ye, H. Poppa, R. Kilaas, and C.
Kisielowski, *Phys. Rev. Lett.* **100**, 017205 (2008).
- 44 R.M. Wang, O. Dmitrieva, M. Farle, G. Dumpich, M. Acet, S. Mejia-Rosales, E. Perez-
Tijerina, M.J. Yacaman, and C. Kisielowski, *J. Phys. Chem. C* **113**, 4395 (2009).
- 45 C. Antoniak et al., *Journ. of Phys: Cond. Mat.* **21**, 336002 (2009).
- 46 O. Šipr, M. Košuth, and H. Ebert, *Phys. Rev. B* **70**, 174423 (2004).
- 47 C. Antoniak, M. Spasova, A. Trunova, K. Fauth, M. Farle, and H. Wende, *Journ. of
Phys.: Conf. Series* **190**, 012118 (2009).
- 48 J.G. Gay and R. Richter, *Phys. Rev. Lett.* **56**, 2728 (1986).
- 49 J.N.W. Karas and L. Fritsche, *J. Chem. Phys. Phys.-Chem. Bio.* **86**, 861 (1989).
- 50 M. Delalande, M.J.F. Guinel, L.F. Allard, A. Delattre, R. Le Bris, Y. Samson, P. Bayle-
Guillemaud, and P. Reiss, *Journ. of Phys. Chem. C* **116**, 6866 (2012)
- 51 M.E. Gruner, *Phys. Status Solidi A* **270**, 1282 (2013).
- 52 C. Antoniak et al., *Nature Commun.* **2**, 528 (2011).
- 53 V. Turkowski, A.Kabir, N. Nayyar, and T.S. Rahman, *Journ. of Chem.* **136**, 114108
(2012).
- 54 V. Turkowski, A.Kabir, N. Nayyar, and T.S. Rahman, *Journ. of Phys.: Cond. Mat.* **22**,
462202 (2010).